RSC Advances

PAPER

View Article Online
View Journal | View Issue

Cite this: *RSC Adv.*, 2026, **16**, 3819

Fluorescent biosensor based cerium-doped carbon quantum dots for albumin detection

Nashwa Ashraf Hafez, Eman Fadl, Shaker Ebrahim, Moataz Soliman and Azza Shokry *

Accurate detection of albumin proteins is crucial for diagnosing different diseases. A fluorescent sensor has been developed using cerium (Ce) doped carbon quantum dots (CQDs) to detect bovine serum albumin (BSA) in blood and urine samples. Pristine CQDs and Ce-CQDs were synthesized through citric acid pyrolysis. CQDs and Ce-CQDs exhibited emission peaks at 415 nm and 426 nm, respectively. Based on the photoluminescence (PL) enhancement of Ce-CQDs resulting from adding BSA, BSA was quantified within two minutes. This biosensor was selective and sensitive towards BSA in the concentrations ranging from 1 to 1000 μM with a high correlation coefficient and a low detection limit of 0.98 μM (6.5 × 10^{-2} g L^{-1}), which meets the requirement well for clinical analysis. The practical usefulness of Ce-CQDs as a fluorescent biosensor was confirmed by accurately quantifying BSA in human serum and urine samples with satisfactory recovery percentages.

Received 29th September 2025
Accepted 23rd December 2025

DOI: 10.1039/d5ra07395b

rsc.li/rsc-advances

1 Introduction

Albumin constitutes 40–60% of the overall proteins in the bloodstream, and it is a carrier for specific fatty acids, drugs, vitamins, steroids, calcium, and hormones. It is crucial to maintain the blood colloid osmotic pressure and prevent fluid leakage from the blood vessels.[1–3] The normal concentration of human serum albumin in blood serum ranges from 35 to 45 g L^{-1}, while in the urine, it is less than 0.2 g L^{-1}.[4–6] Having an abnormal level of albumin in the body can lead to severe illnesses like heart disease, kidney disease, diabetes, renal disorders, and liver cirrhosis.[6,7] The structural similarity and homology between bovine serum albumin (BSA) and human serum albumin are very high. Because of this, BSA is often used as a model protein in various fields instead of human serum albumin. BSA, like human serum albumin, is a globular protein shaped like a heart. It is made up of 583 amino acids and has a molecular weight of 66.4 kDa. The structure of BSA is stabilized by 17 disulfide bridges formed by 35 cysteine (Cys) amino acids.[6–9]

Various techniques, such as piezoelectric quartz crystal impedance,[10] Raman,[11] near-infrared emissive fluorophores,[12] molecularly imprinted and surface plasmon resonance[13] have been used to identify and measure bovine serum albumin. However, these techniques are both time-consuming and costly. Additionally, they involve complex procedures and have a limited range of accuracy.[14] On the contrary, the fluorescence technique has high sensitivity, quick response time, and good selectivity.[15]

Carbon quantum dots (CQDs) are carbon nanoparticles smaller than 10 nm that exhibit high photoluminescence quantum yields, tunable multicolor emission, excellent water solubility, chemical stability, low toxicity, and biocompatibility.[16–20] Their optical properties are governed by core graphitic nitrogen and surface functional groups, including controlled fluorescence blinking, fast core-localized emission dynamics, chirality, and two-photon absorption. These characteristics enable applications in bioimaging, single-molecule and super-resolution microscopy, FRET/RET-based biosensing, chiral sensing, optoelectronic devices, and photocatalysis.[21–29] Understanding surface–core interactions and carrier dynamics provides a foundation for designing next-generation C-Dot-based materials for biomedical, sensing, and photonic technologies.[30]

Lanthanide-doped nanomaterials possess tunable visible and near-infrared emission, long photoluminescence lifetimes, high photostability, and upconversion luminescence.[31,32] Cerium (Ce^{3+}/Ce^{4+}) plays a key role as a sensitizer, enhancing energy transfer to other lanthanides and increasing overall luminescence efficiency.[33,34] These nanoparticles are surface-functionalizable for biocompatibility and targeting, enabling applications in bioimaging, NIR-II image-guided surgery, molecular sensing, luminescent labeling, optoelectronics, and therapeutic strategies such as photothermal and photodynamic therapies. Their tunable optical properties, nanoscale size, chemical stability, and enhanced luminescence make them versatile platforms for both diagnostic and therapeutic biomedical applications.[35–39]

Department of Materials Science, Institute of Graduate Studies and Research, Alexandria University, P.O. Box 832, Alexandria, Egypt. E-mail: azzashokry@alexu.edu.eg

To the best of our knowledge, this is the first study to employ Ce-doped carbon quantum dots (Ce-CQDs) synthesized *via* the pyrolysis method as a photoluminescent probe for the selective detection of BSA. The novelty of this work lies in establishing a simple and efficient synthesis route that produces highly luminescent Ce-CQDs, and demonstrating their remarkable selectivity and sensitivity toward BSA in aqueous media across a broad concentration range (1–1000 μM), with the detection limit that satisfies clinical albumin-testing requirements. In addition, this research provides new insight into the PL enhancement mechanism based on the interaction between Ce-CQDs and BSA, and validates the practical applicability of the sensor through successful detection of BSA in real human serum and urine samples.

2 Experimental

2.1. Chemicals and reagents

Citric acid anhydrous (99.5%) was purchased from LOBA Chemie, India. Cerium(III) nitrate hexahydrate (99%), Bovine serum albumin (BSA) (≥96%), and acetone (99.0%) were provided by Sigma Aldrich, United States. Ammonia solution (30–33%) was supplied by Piochem, Egypt. Glycerol (99.5%) was delivered by MP Biomedicals, France. A dialysis bag (1 kDa molecular weight) was purchased from Millipore-Sigma. Cobalt(II) chloride hexahydrate and copper(II) sulfate pentahydrate were purchased from Fisher Scientific, United Kingdom. Nickel(II) nitrate hexahydrate (99%), sodium dihydrogen orthophosphate extra pure (Dihydrate) (98%), and disodium hydrogen phosphate dihydrate (99%) were obtained from LOBA Chemie, India. L-cysteine (98+) was obtained from Acros Organics, Belgium. Glycine (99%) was obtained from BDH Chemicals Ltd, England. Dopamine 200 mg/5 mL was purchased from Eimc, Egypt. Human serum and urine samples were obtained from a local medical laboratory. Mission Expert Urinalysis Strips were purchased from a local medical laboratory.

2.2. Synthesis of pristine CQDs

The pristine CQDs were prepared using pyrolysis of citric acid (CA) as mentioned before in our recently published article.[40] Two grams of CA were added to a glass beaker and placed in a previously heated glycerol bath at 170 °C for five minutes at the same temperature. The CA turned into a liquid five minutes after heating began. As the heating continued, the liquid's color shifted from clear to light yellow to orange within half an hour. Then, 50 mL of deionized water was added to the orange liquid and vigorously stirred until fully dissolved. The CQDs solution was neutralized to pH 7.0 with ammonia solution. The resulting CQD solution was centrifuged for 30 min at 5000 rpm for 24 h before dialysis. The solution was then dialyzed using a 1000 Da molecular weight dialysis bag and deionized water for 48 h to purify the orange CQD solution. The solution was dried at 140 °C on a hot plate for 3 hours to obtain CQDs powder.

2.3. Synthesis of Ce-CQDs

The Ce-CQDs were synthesized by gradually introducing 0.64 g of cerium(III) nitrate hexahydrate into the previously prepared CQDs under vigorous stirring for 10 minutes at room temperature. This mixture turned into a transparent orange solution of Ce-CQDs as presented in Scheme (1). The Ce-CQDs solution was dialyzed in the same manner as mentioned for the CQDs to remove excess Ce salt. To obtain the Ce-CQDs in powder form, the orange solution was dried on a hot plate at 140 °C for 3 hours.

2.4. Characterization techniques

The optical properties of CQDs and Ce-CQDs were investigated using a UV-Visible spectrophotometer (Evolution 300, Thermo Scientific, USA). The P spectra data were obtained in the 300–600 nm range using a fluorescence spectrophotometer, PerkinElmer (model LS-55, United Kingdom). Structural properties were confirmed by Fourier transform infrared spectroscopy (FTIR) (BX 11- LX 18-5255, PerkinElmer, United Kingdom), Raman spectroscopy (WiTec, 300R alpha, Germany) with Ar ion laser λ = 785 nm, X-ray diffraction (XRD)(Bruker-AXS D8 Discover, Germany), X-ray photoelectron spectroscopy (XPS) (Thermo Fisher Scientific, USA). Morphology, particle size, and

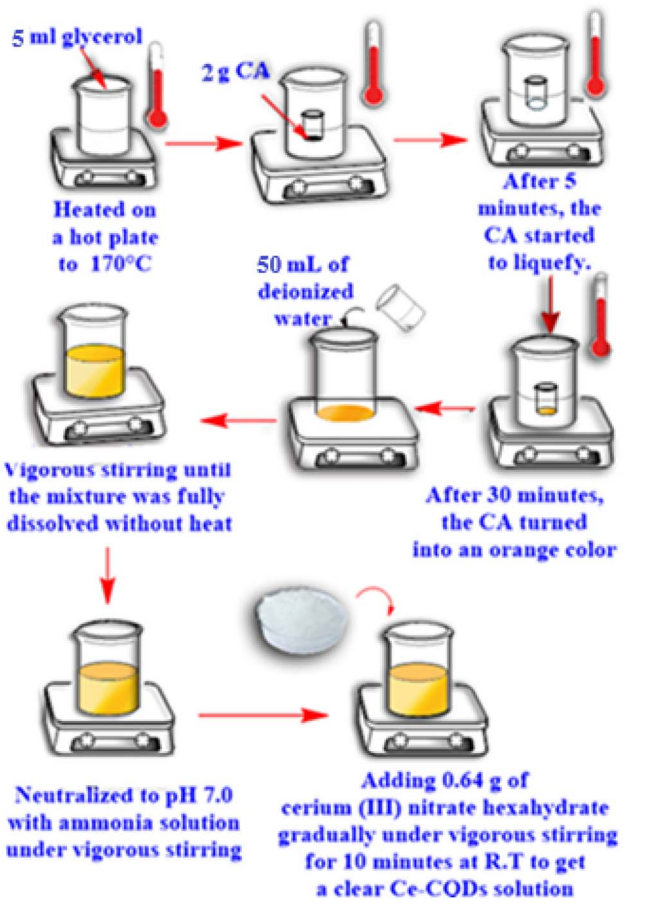

Scheme 1 Schematic illustration of the synthesis steps of Ce-CQDs at room temperature (R.T.) *via* pyrolysis of citric acid (CA).

elemental analysis were investigated using high resolution transmission electron microscopy (HRTEM) coupled with Energy Dispersive X-ray Spectroscopy (EDX) (JEOL, JEM-2100 LaB6, Thermo Fisher Scientific, USA). Surface charges were measured by Zeta Potential (Zetasizer Nano ZS, Malvern).

2.5. Procedure for BSA detection using Ce-CQDs photoluminescence measurements

For BSA detection experiments, a stock solution of 2 mM of BSA was made by dissolving 3.325 g of BSA in 25 mL of distilled water. To assess the sensitivity and linearity, different concentrations of BSA ranging from 1 to 1000 μM from the stock solution were mixed with 0.6 mL of Ce-CQDs and 1 mL of phosphate-buffered saline (PBS) with a pH of 7.3 ± 0.1. This mixture was then subjected to a vortex mixer and incubated at room temperature for 2 minutes. Afterwards, the PL of the Ce-CQDs was measured at an excitation wavelength (λ_{ex}) of 310 nm. The highest intensity of PL observed at 426 nm was utilized to measure the concentration of BSA. The optimal experimental detection conditions were determined by investigating how the solution pH and the response time between Ce-CQDs and BSA affected the results. The selectivity of Ce-CQDs for BSA has been examined by observing the alterations in PL intensity while using 400 μM of different substances such as Co(II), Cu(II), L-cysteine, glycine, Ni(II), acetone, and dopamine. We conducted three repetitions for each measurement. Ultimately, we utilized Ce-CQDs to detect BSA in real human serum and urine samples. To optimize the analytical parameters, we relied on the slope of the calibration curve, as indicated in eqn (1):[41]

$$(F - F_0)/F_0 = a\,C_{BSA} + b \quad (1)$$

The PL intensity of Ce-CQDs in the presence and absence of BSA is indicated as F and F_0, respectively. The concentration of BSA is represented as C_{BSA}, and the slope and intercept of the calibration curve are denoted as a and b, respectively. The PL flouresence effect (FE) was calculated using eqn (2):[42]

$$FE = (F - F_0)/F_0 \quad (2)$$

Eqn (3) was used to establish the limit of detection (LOD), the lowest concentration of BSA that can be detected:[43]

$$LOD = \frac{3SD}{S} \quad (3)$$

SD and S refer to the standard deviation and slope of the calibration curve.

2.6. Procedure for BSA quantification in real serum samples

Two healthy adult volunteers provided blood samples collected at a local clinical laboratory. The samples were then centrifuged for 5 minutes to separate the serum from the blood. These serum samples were diluted 100-fold with 0.1 M PBS buffer solution at a pH of 7.3 ± 0.1. A standard method was employed to determine the BSA concentration using an automated spectrophotometer (CS-T240 AUTO-Chemistry Analyzer). The samples were placed in the spectrophotometer, and the level of light absorption was measured for each sample. The diluted blood serum samples with a known quantity of BSA were examined using the standard addition method. The BSA detection procedure by Ce-CQDs was described as follows: 0.6 mL of Ce-CQDs solution was mixed with different concentrations of BSA from 100 to 1000 μM and 1 mL PBS. The mixture was then incubated for 2 min, followed by PL measurements at λ_{ex} of 310 nm.[1,44] Eqn (4) was utilized to calculate the recovery percentage.[45]

$$\text{Recovery}\% = (\text{concentration found/concentration added}) \times 100\% \quad (4)$$

To detect BSA levels in a local clinical laboratory, set the wavelength of the spectrophotometer to 623 nm (alternative: 578 nm). Allow the reagent, standards, and samples to reach room temperature (20–25 °C). Label three tubes as: Blank, Standard, and Sample. Pipette the following volumes into each tube: Blank: 1.0 mL Reagent + 10 μL Distilled Water, Standard: 1.0 mL Reagent + 10 μL Albumin Standard, and Sample: 1.0 mL Reagent + 10 μL Serum Sample. Mix gently and incubate all tubes for 5 minutes at room temperature (20–25 °C). The absorbance is measured automatically at 623 nm. The analyzer calculates the albumin concentration automatically using the built-in calibration curve or standard factor. The final result appears directly on the screen in g dL^{-1} (or g L^{-1}, depending on the device settings).

2.7. Procedure for BSA quantification in urine samples

Three healthy adult volunteers provided urine samples that were collected at a local clinical laboratory. Before the samples were centrifuged for 3 minutes to eliminate undesired precipitates, the urine sample was diluted 20-fold with PBS buffer. A known quantity of BSA was added to the diluted samples. To detect BSA levels in a local clinical laboratory by immersing the urinalysis strips in urine and then observing them after 2 minutes. The test strips commonly used can detect concentrations of urinary protein ranging from 0.15 to 20 g L^{-1} and categorize them into 5–6 categories: Negative, trace, +1, +2, +3, and +4. The most frequently observed concentration of protein on the test strip falls within the range of 0.15–10 g L^{-1}. The protein test pad on the strip provides an approximate measurement of the amount of albumin present in the urine. According to the reference range indicated by the strips, a concentration of 3 g L^{-1} (45 μM) (+++) indicates a significantly elevated level of albumin, 1 g L^{-1} (15 μM) (++) indicates an increased level, and 0.3 g L^{-1} (4.5 μM) (+) indicates a slightly increased level.[46] The BSA concentration was measured by recording the PL response of the proposed Ce-CQDs sensor. The % recovery and the relative standard deviation (RSD) were also calculated.[1]

2.8. Ethical approval

All experiments were performed in accordance with the Guidelines of Ethical Standards of Scientific Research, and

experiments were approved by the ethics committee at Alexandria University. Informed consents were obtained from human participants of this study.

3 Results and discussion

3.1. Characterization of CQDs and Ce-CQDs

Our previous research[40] presented and discussed the characterization results of pristine CQDs and CQDs-Ce, including their structure, crystallinity, and morphological properties. FT-IR spectra in Fig. S1a (S: SI) presented the distinctive functional groups of CQDs and Ce-CQDs. Raman spectra in Fig. S1b showed a slight rise in the intensities of the (I_D/I_G) ratio, from 0.86 in CQDs to 0.87 in the Ce-CQDs. The intense G-band, when compared to the D-band, highlights the presence of carbon nanomaterials in pristine CQDs. These CQDs primarily consist of sp^2 carbons with a few sp^3 hybrid carbons. The XRD patterns in Fig. S2 revealed that the crystalline sizes of CQDs and Ce-CQDs are 0.27 nm and 0.99 nm, respectively, according to Debye–Scherrer's equation. The EDX analysis (Fig. S3) of CQDs displayed only C and O elements, and the characteristic peaks of C, O, and Ce elements in Ce-CQDs. Nitrogen is not detected in the EDX spectrum of Ce-CQDs, which may be due to the low quantity of nitrogen. XPS analysis in Fig. S4 proved the existence of C, N, and O elements of pristine CQDs and C, O, N, and Ce elements of Ce-CQDs. The zeta potential value of Ce-CQDs (−22.4 mV) was greater than CQDs (−10.9 mV), which confirmed the higher stability of Ce-CQDs than of pristine CQDs, as shown in Fig. S5. The HRTEM images (Fig. S6) confirmed that CQDs and Ce-CQDs are almost spherical agglomerates with a lattice spacing of about 0.2 nm, and their particle size ranges from 1.4 nm to 7.8 nm. Ce-CQDs are quasi-spherical in shape, uniformly distributed dots with a lattice spacing of 0.2 nm, and their diameter size is between 3.7 and 9.6 nm. The electron diffraction patterns confirmed that CQDs and Ce-CQD_S are polycrystalline materials.

3.2. Optical properties of Ce-CQDs

Our previous research[40] presented and discussed that the most intense emission occurs at the wavelength of 310 nm. These findings demonstrate that the emission characteristics of Ce-CQDs are dependent on the wavelength of excitation. One possible explanation for this behavior may be attributed to the varying sizes of particles and the configuration of surface states.[47] Our previous research[40] presented and discussed the ideal concentration for adding Ce to pristine CQDs as 15% due to the ability of Ce to enhance the surface defects of CQDs and improve the intensity of emitted light.[48,49] Schematic presentation of the effect of Ce(III) on the PL enhancement mechanism of CQDs is shown in Fig. 1(a).[50] When pristine CQDs (2 g L^{-1}) are excited with 310 nm, the valence electrons of the carbon atoms are promoted to an excited state. This unstable, excited state relaxes through vibrational energy exchange, returning to the

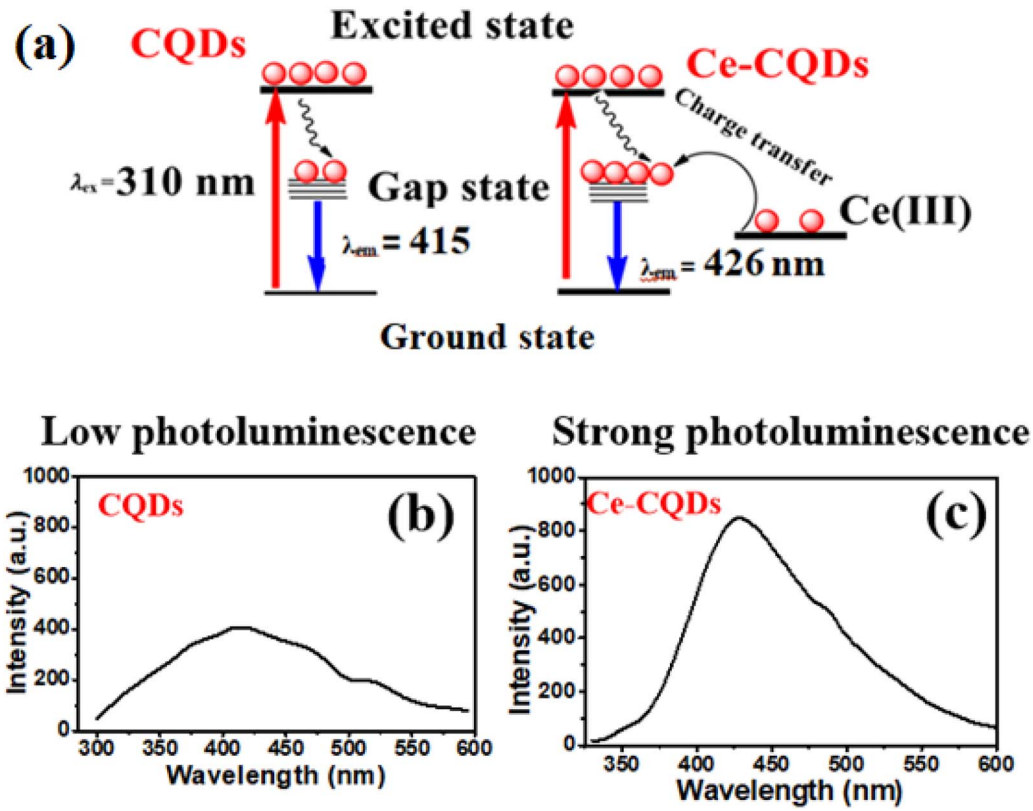

Fig. 1 Schematic presentation of the effect of Ce(III) on the PL enhancement mechanism of CQDs (a), PL spectra of 2 g L^{-1} of CQDs (b), and 2 g L^{-1} of Ce-CQDs (c) excited at λ_{ex} = 310 nm, showing enhanced emission intensity compared to undoped CQDs.

same energy level. The remaining energy is then released as optical radiation, resulting in low photoluminescence at 415 nm as shown in Fig. 1(b). When Ce is added, the carboxyl groups in the CQDs coordinate with Ce(III) ions, providing additional electrons to the CQDs. Additionally, Ce(III) provides coordination sites for –COOH groups on the surface of CQDs, which passivates dangling surface carboxyl bonds,[51] suppresses non-radiative energy losses, and enhances photoluminescence for Ce-CQDs (2 g L^{-1}) compared to pristine CQDs, as shown in Fig. 1(c).

The stability of CQDs and Ce-CQDs is studied by recording their UV-Vis and PL emission spectra over 24 weeks, as shown in Fig. 2. The UV-Vis absorption spectra of CQDs (2 g L^{-1}) and Ce-CQDs (1 g L^{-1}) shown in (Fig. 2a and c, respectively) display a strong peak at 230.2 nm due to π–π transition of the C=C bond[14,52] and a weak shoulder at 346.6 nm associated with the n–π* transition of the C=O bond. It is noted that these peaks appear in Ce-CQDs with a slight blue shift in the peak positions to 229.7 nm and 342.1 nm, respectively. It is found that the intensity of the absorption peak located at 230.2 nm in CQDs dramatically decreased by 58.8% in 20 weeks (Fig. 2(a)). Ce-CQDs demonstrated greater stability over CQDs with only a 14.5% decrease in peak intensity after 24 weeks (Fig. 2(c)). The PL emission spectra of CQDs (2 g L^{-1}) and Ce-CQDs (1 g L^{-1}) over 24 weeks in (Fig. 2b and d, respectively) show that Ce-CQDs are more stable than CQDs, with a decrease of only 7.1% in intensity after 24 weeks. In addition, the emission peak of Ce-CQDs is narrower and red-shifted to 426 nm compared to

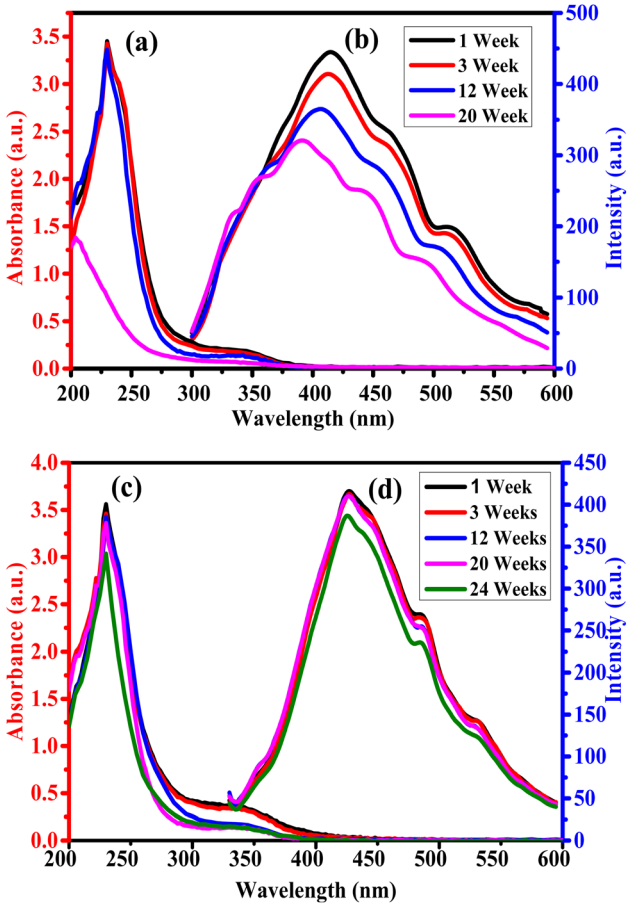

Fig. 2 UV-Vis absorption spectra of CQDs (2 g L^{-1}) (a), PL spectra of CQDs (2 g L^{-1}) (b), UV-Vis absorption spectra of Ce-CQDs (1 g L^{-1}) (c), and PL spectra of Ce-CQDs (1 g L^{-1}) (d), showing enhanced emission intensity and stability over time at λ_{ex} = 310 nm.

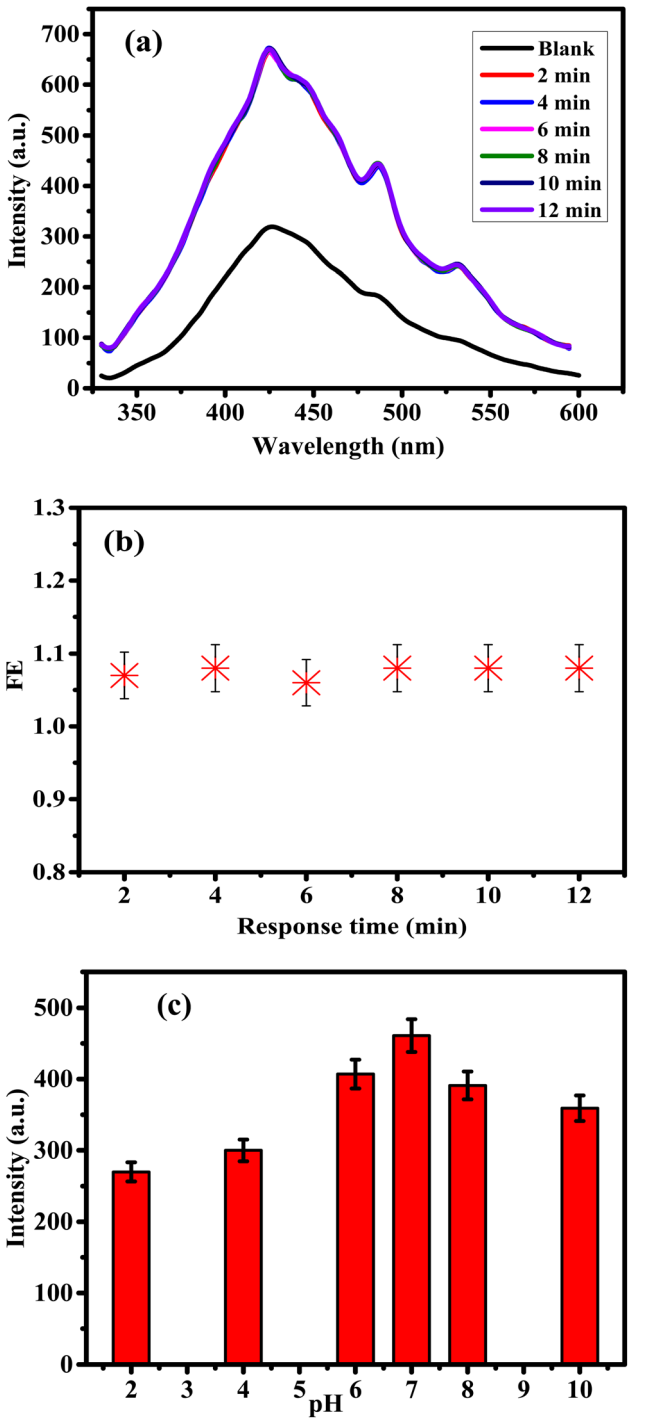

Fig. 3 PL intensity of Ce-CQDs in the presence of 200 μM BSA at different time intervals (a), fluorescence enhancement (FE = $(F - F_0)/F_0$) *versus* response time (b), and PL intensity of Ce-CQDs as a function of pH (2 – 10) using 0.1 M PBS (c) at λ_{ex} = 310 nm.

pristine CQDs (415 nm). These peak shifts in both UV-Vis and PL spectra indicate a strong interaction between CQDs and cerium.[53] These results suggest that Ce-CQDs are a better choice for sensing applications than pristine CQDs.

3.3. The optical performance of Ce-CQDs for BSA detection

The intensity of light emitted by Ce-CQDs is a key characteristic of their use in detecting BSA. The effect of the response time (ranging from 2 to 12 minutes) on the PL intensity and FE of Ce-CQDs mixed with 200 μM BSA with Ce-CQDs is investigated, as shown in (Fig. 3a and b, respectively). It is observed that the PL intensity of Ce-CQDs in the absence of BSA (blank) is enhanced rapidly within approximately 2 minutes after the addition of 200 μM BSA and then remains constant. The results suggest that Ce-CQDs have a strong ability to react with BSA, and they also possess excellent stability.[54]

The influence of pH on the PL intensity of Ce-CQDs was investigated within a pH range of 2 to 10 using 0.1 M PBS

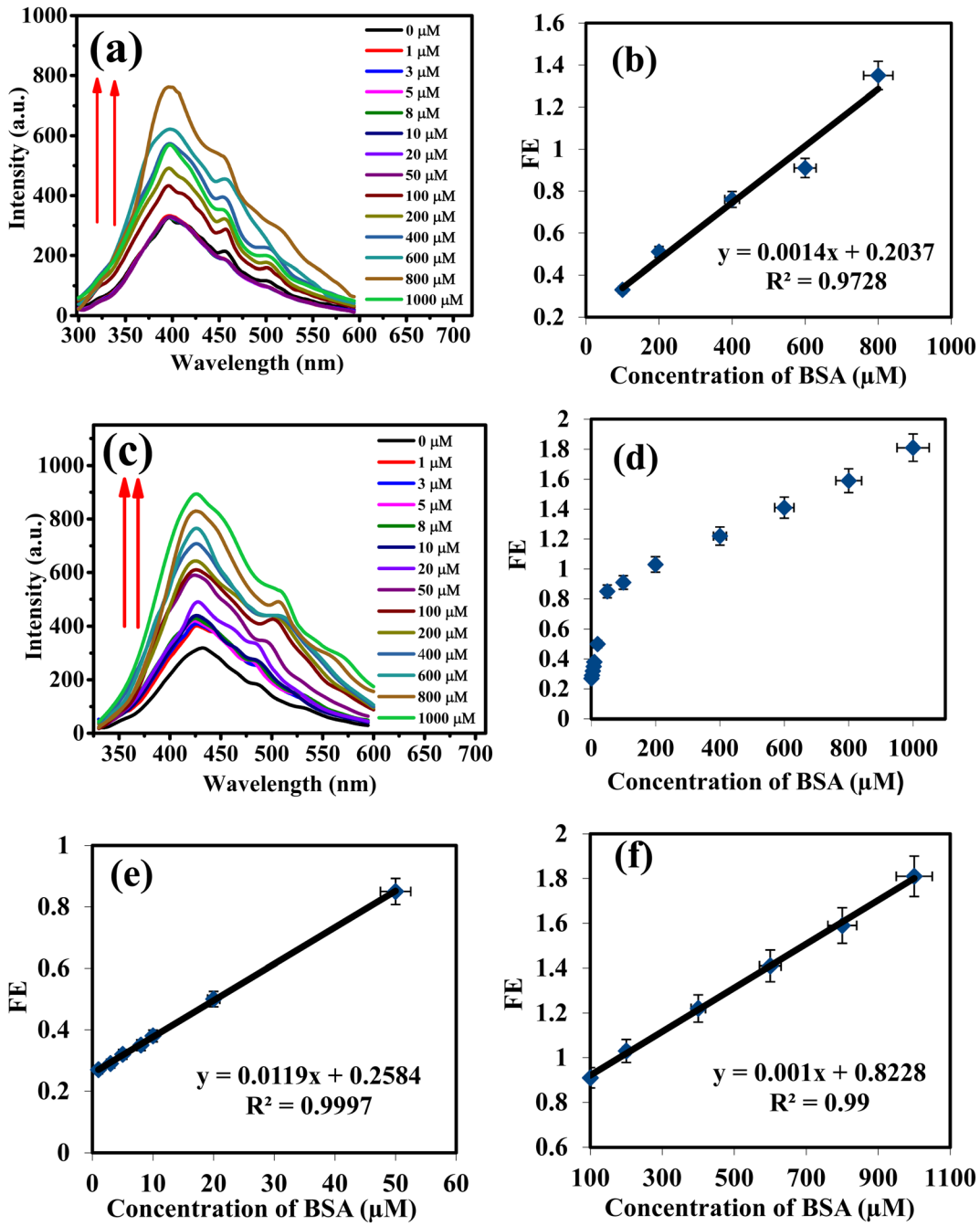

Fig. 4 PL spectra of CQDs with varying concentrations of BSA (1 μM–1000 μM) (a), FE *versus* BSA concentration from 100 to 800 μM (b), PL spectra of Ce-CQDs with varying concentrations of BSA (1 μM–1000 μM) (c), FE *versus* BSA concentration from (d) 1 to 1000 μM, (e) 1 to 50 μM, and (f) 100 to 1000 μM at λ_{ex} = 310 nm.

(Fig. 3(c)). An increase in solution pH from 2 to 7 resulted in an enhancement of Ce-CQDs PL intensity. In highly acidic conditions, protonation of amine groups on the C-dot surface likely leads to aggregation and altered light emission. At neutral pH 7, maximum PL intensity was observed, possibly due to partial ionization of carboxylic and hydroxyl groups. This creates a charge on the surface, causing electrostatic repulsion, which prevents aggregation and quenches photoluminescence.[55] Further increasing the pH (>7) gradually decreased PL intensity. In alkaline media, deprotonation of amino and carboxylic groups on CQDs generates negative surface charges and forms anionic double layers, disrupting Ce-CQDs fluorescence.[56] Considering the pH range of human serum (approximately 7.35–7.45), pH 7.3 ± 0.1 was selected for BSA detection.[40]

3.4. Sensitivity and limit of detection of cerium-doped pristine CQDs albumin sensor

To evaluate the effectiveness of CQDs and Ce-CQDs for detecting BSA, crucial factors like the limit of detection (LOD) and sensitivity are measured. The impact of BSA concentrations ranging from 1–1000 μM in an aqueous solution on the PL spectra of pristine CQDs and Ce-CQDs is examined, as shown in Fig. 4(a and b).

The addition of different concertation of BSA to the pristine CQDs as shown in Fig. 4(a), leads to no effect observed for concentrations from (1–50 μM) and an increase in the peak intensity of the PL for concentrations from (100–800 μM) with no shift in the peak position then decrease in the peak intensity of

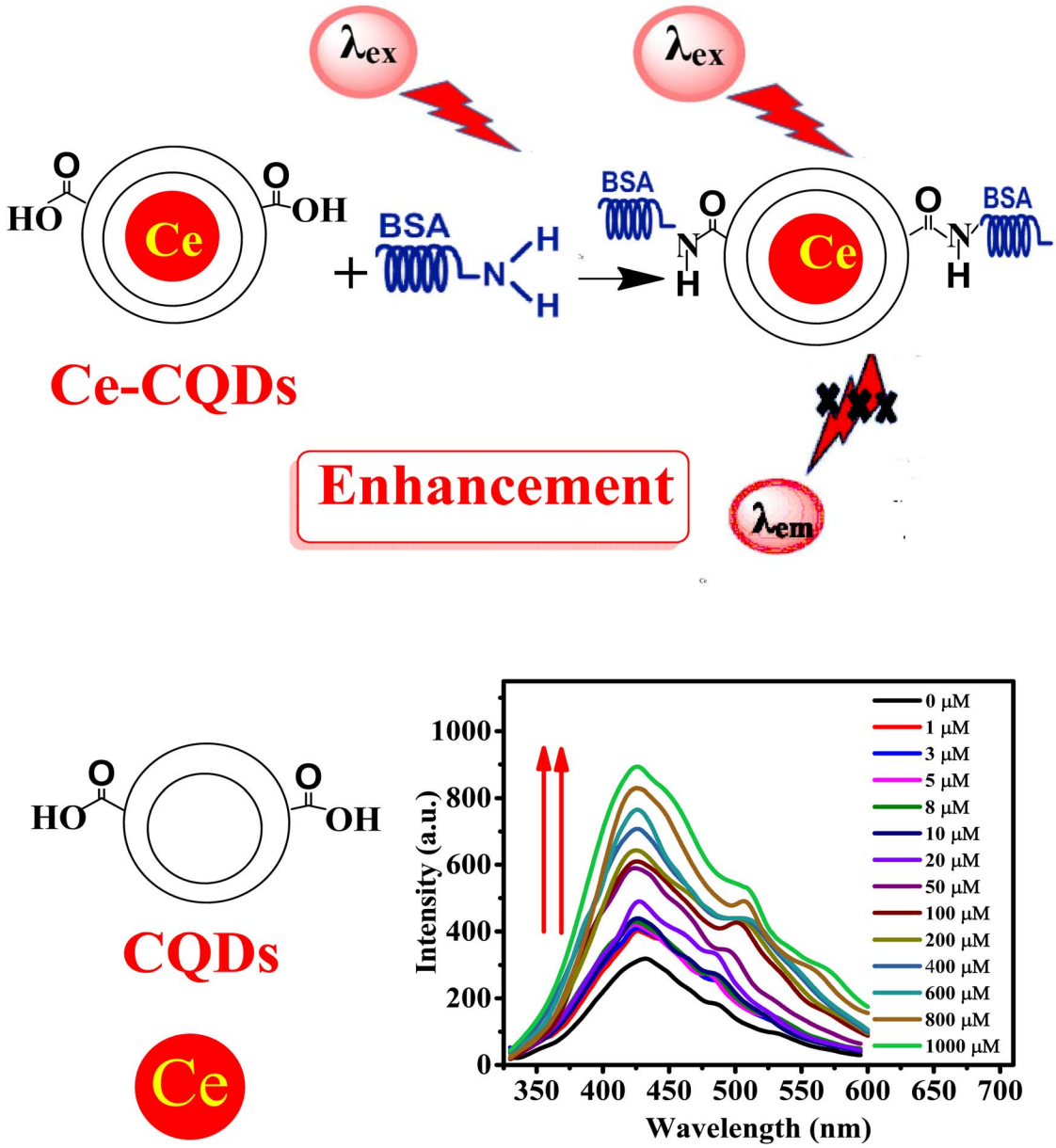

Fig. 5 Schematic illustration of the sensing mechanism of BSA using Ce-CQDs at λ_{ex} = 310 nm.

the PL at 1000 μM. In Fig. 4(b) linear region can be observed for different BSA concentration ranges (100–800) μM ($R^2 = 0.9728$), with sensitivity (represented by the slopes of the calibration lines) and limit of detection (LOD) are 0.0014 and 182.5, respectively.

To verify the effectiveness of the Ce-CQDs sensor in detecting BSA, different concentrations of BSA solutions (ranging from 1 to 1000 μM), as shown in Fig. 4, were prepared and mixed with the suggested sensor under optimal conditions. Fig. 4(c) shows the emission spectra of Ce-CQDs at various concentrations of BSA, ranging from 1 to 1000 μM. As the concentration of BSA increased, the intensity of the emission peak also increased proportionally, with a slight blue shift in the peak position by 6 nm. This shift suggests that the size of the QDs has decreased because the interaction between Ce-CQDs and BSA has been enhanced.[56–58] The efficiency of PL enhancement in Ce-CQDs depends on the concentration of BSA, as depicted in Fig. 4(d). In Fig. 4(e and f), two linear regions can be observed for different BSA concentration ranges: 1–50 μM ($R^2 = 0.9997$), and 100–1000 μM ($R^2 = 0.99$) with different sensitivities of 0.0119 and 0.001 μM related to the range of detection, and a low LOD of 0.98 μM, respectively, as revealed in Fig. 4(f).

3.5. Sensing mechanism of BSA

The suggested interaction process between Ce-CQDs and BSA is depicted in Fig. 5. Bovine serum albumin interacts with Ce-CQDs through the surface carboxyl (–COOH) groups and the amine ($–NH_2$) groups of BSA. This interaction forms stable bonds that passivate the surface by reducing the number of dangling carboxylic bonds. Such passivation minimizes non-radiative relaxation pathways and enhances the photoluminescence efficiency of both CQDs and Ce-CQDs.[51] Additionally, the holes at the valence band of the QDs have higher energy than a molecular orbital on the ligand. As a result, the abundant electrons in BSA act as electron donors and transfer to the QDs, thereby increasing the QD PL intensity.[56,59] Additionally, mixed valence (Ce^{3+} and Ce^{4+}), which provides additional coordination sites for $–NH_2$ and –COOH groups on the surface of BSA, enhances selective binding.[60]

3.6. Identification of BSA by Ce-CQDs

The selectivity of a biosensor is determined by its ability to identify BSA among analytes that could potentially interfere

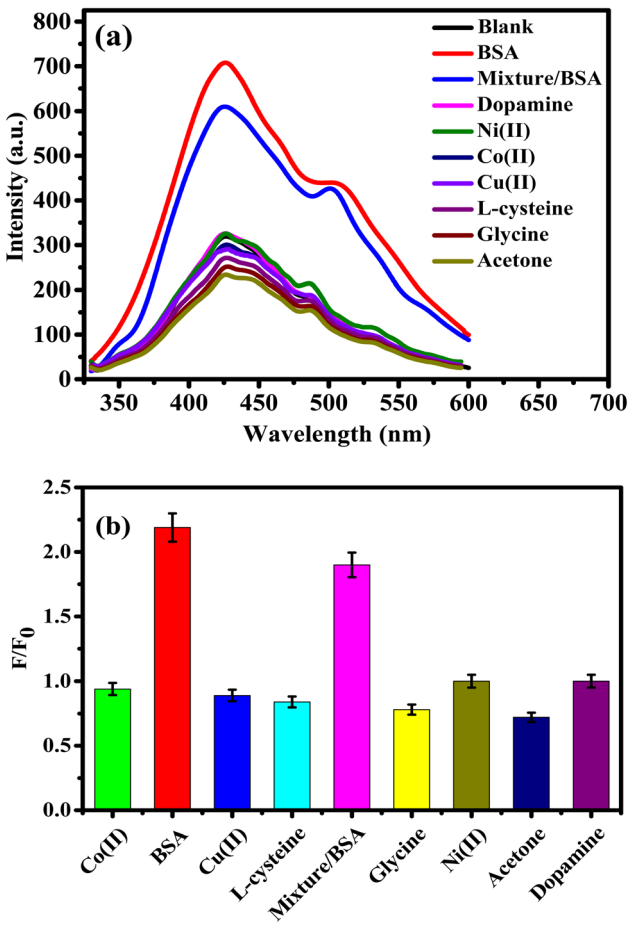

Fig. 6 PL intensity of Ce-CQDs in the presence of 400 μM of various interfering analytes (a) and relative fluorescence intensity (F/F_0) of Ce-CQDs *versus* 400 μM of different interfering substances, $\lambda_{ex} = 310$ nm (b).

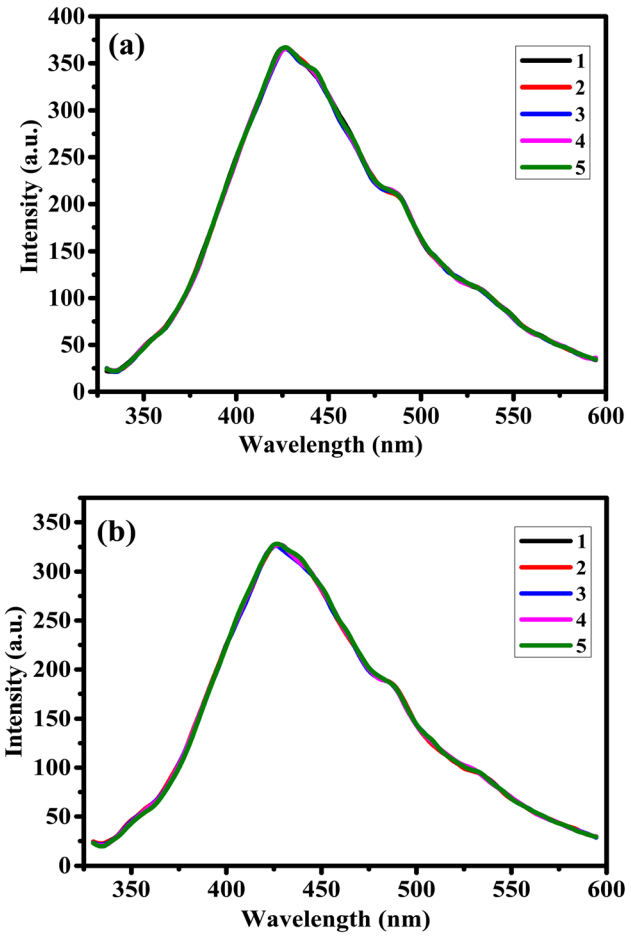

Fig. 7 The repeatability of Ce-CQDs for 5 independent PL measurements of a sample containing 3 μM BSA (a) and the reproducibility of Ce-CQDs for PL measurements of 5 different samples containing 1 μM BSA (b), $\lambda_{ex} = 310$ nm.

with the detection process, including albumin, dopamine, Co(II), Ni(II), Cu(II), L-cysteine, glycine, acetone, and their mixture/BSA that already co-exist with BSA in the blood serum. Fig. 6 shows the PL spectra and relative PL intensity (F/F_0) of Ce-CQDs after mixing with 400 μM of different interferents. Results revealed that dopamine and Ni(II) do not affect the PL response of Ce-CQDs. On the other hand, Co(II), Cu(II), L-cysteine, glycine, and acetone have a moderate quenching effect on the PL response. It was observed that BSA significantly enhanced the fluorescence of Ce-CQDs, while other ions had a minimal effect, as shown in Fig. 6(a). To study the interference of various ions with BSA, a sample containing a mixture of 400 μM of each ion was prepared with the Ce-CQDs in the presence of 400 μM BSA. The slight change in relative PL intensity (F/F_0) of the Ce-CQDs from 2.2 to 1.9 in Fig. 6(b), caused by interfering ions, was minimal compared to the change observed in a sample containing only BSA. These results indicate that various metal ions and biomolecules do not greatly affect the PL intensity of Ce-CQDs, highlighting their exceptional selectivity for detecting BSA, and can be used as a sensor in real samples.

3.7. Repeatability and reproducibility

To assess repeatability, five consecutive PL measurements were performed on the same Ce-CQDs sample containing 3 μM BSA (Fig. 7(a)). A low relative standard deviation (RSD) of 0.15% was calculated. Reproducibility was evaluated by measuring the PL intensity of Ce-CQDs in five independently prepared 1 μM BSA solutions. As shown in Fig. 7(b), the RSD was 0.43%. These results demonstrate the high repeatability and reproducibility of the Ce-CQDs biosensor, making it suitable for reliable and consistent investigations.

3.8. Detection of BSA in real serum samples using Ce-CQDs

Table S1 compares BSA concentrations determined using the Ce-CQDs sensor, analyzed with the standard addition method shown in Fig. S7, to those obtained from a local clinical laboratory. The close agreement between these results demonstrates the Ce-CQDs sensor's sensitivity, accuracy, and quantitative capabilities for BSA detection in biological samples.

3.9. Detection of BSA using Ce-CQDs in urine samples

The detection of BSA in three urine samples was performed using the Ce-CQDs sensor (Fig. 8). For comparison, BSA levels were measured using Mission Expert Urinalysis Strips at a local medical laboratory. Each urine sample was subjected to three fluorescence measurements. The calibration curve presented in Fig. 4(e) was then used to determine the BSA concentration in each sample.

Table S2 shows the BSA concentration determined using the proposed sensor and the clinical data provided by the laboratory for each sample. The recovery percentages for the Ce-CQDs sensor ranged from 93.7% to 106%, and the RSD ranged from 0.13% to 0.207%. These results demonstrate that the prepared Ce-CQDs sensor is accurate and efficient for determining BSA concentrations in urine samples.

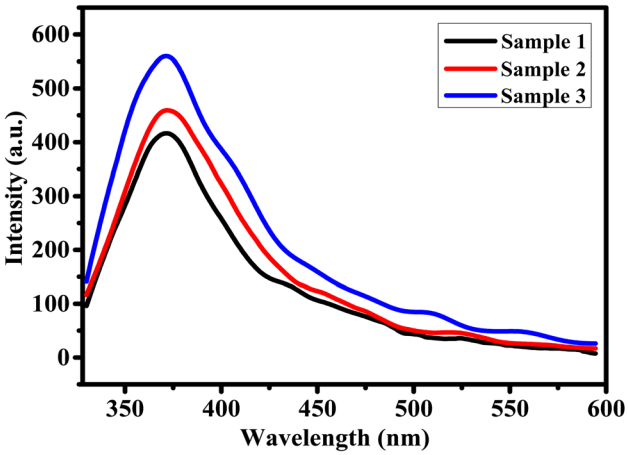

Fig. 8 PL spectra of human urine samples at λ_{ex} = 310 nm.

4 Conclusion

Photoluminescent CQDs were developed using pyrolysis method and were doped with different concentrations of cerium (5%, 10%, 15%, 20%, and 25%). Among these concentrations, 15% was found to be the most effective. The Ce-CQDs sensor was then used as biosensor sensor for the detection of BSA. The sensor was optimized by adjusting the measurement incubation time and pH. Ce-CQDs exhibited good stability, selectivity, and sensitivity toward BSA, with a detection limit of 0.98 μM. BSA enhanced the PL intensity of Ce-CQDs due to the interaction between the carboxylic groups of Ce-CQDs and the NH_2 of BSA. The applicability of the sensor was tested by analyzing BSA in human serum and urine samples, and satisfactory recovery rates (98.3–102.5%), RSD (0.267–0.251%), recovery% (94.9–106.4%), and RSD (0.133–0.207%) were achieved, respectively. We believe that Ce-CQDs can be useful for the detection of BSA in real blood and urine samples.

Author contributions

Nashwa Ashraf Hafez: writing – original draft, methodology, data curation. Eman Fadl: methodology, supervision. Shaker Ebrahim: review & editing, supervision, methodology, conceptualization. Moataz Soliman: review & editing, supervision, conceptualization. Azza Shokry: writing – review & editing, supervision, methodology, conceptualization.

Conflicts of interest

The authors declare that they have no known competing financial interests or personal relationships that could have appeared to influence the work reported in this paper.

Data availability

Data will be available on request.

Supplementary information (SI) is available. See DOI: https://doi.org/10.1039/d5ra07395b.

References

1 S. Dhanshri, S. Vardhan and S. K. Sahoo, *Methods*, 2022, **206**, 69–76.
2 A. Jahanban-Esfahlan, L. Roufegarinejad, R. Jahanban-Esfahlan, M. Tabibiazar and R. Amarowicz, *Talanta*, 2020, **207**, 120317.
3 L. Roufegarinejad, A. Jahanban-Esfahlan, S. Sajed-Amin, V. Panahi-Azar and M. Tabibiazar, *J. Mol. Recognit.*, 2018, **31**(7), e2704.
4 R. Narayan and S. Singh, *J. Clin. Diagn. Res.*, 2021, **15**(5), SR01–SR02.
5 U. Saeed, B. Fatima, D. Hussain, R. Ashiq, M. N. Ashiq and M. Najam-ul-Haq, *J. Electroanal. Chem.*, 2022, **906**, 115999.
6 L. Wang and L. Zhao, *Colloids Surf., A*, 2022, **632**, 127843.
7 A. Jahanban-Esfahlan, L. Roufegarinejad, M. Tabibiazar, J. M. Lorenzo and R. Amarowicz, *Pol. J. Food Nutr. Sci.*, 2021, **71**, 69–77.
8 A. Jahanban-Esfahlan and V. Panahi-Azar, *Food Chem.*, 2016, **202**, 426–431.
9 T. Topală, A. Bodoki, L. Oprean and R. Oprean, *Clujul Med.*, 2014, **87**(4), 215.
10 Y. Cai, F. Yin, Q. Xie, Y. Zhang and S. Yao, *Microchem. J.*, 2001, **68**, 71–76.
11 J. L. Flores-Guerrero, A. Muñoz-Morales, F. Narea-Jimenez, R. Perez-Fuentes, E. Torres-Rasgado, G. Ruiz-Vivanco, N. Gonzalez-Viveros and J. Castro-Ramos, *Diagnostics*, 2020, **10**(3), 141.
12 R. Choudhury, S. R. Patel and A. Ghosh, *J. Photochem. Photobiol., A*, 2019, **376**, 100–107.
13 A. Araz, *Turk. J. Chem.*, 2022, **46**(2), 487–498.
14 S. Samanta, S. Halder and G. Das, *Anal. Chem.*, 2018, **90**(12), 7561–7568.
15 X. Fu, X. Fu, Q. Wang, L. Sheng, X. Huang, M. Ma and Z. Cai, *Int. J. Biol. Macromol.*, 2017, **103**, 1155–1161.
16 G. Paramasivam, V. V. Palem, S. Meenakshy, L. K. Suresh, M. Gangopadhyay, S. Antherjanam and A. K. Sundramoorthy, *Colloids Surf., B*, 2024, **241**, 114032.
17 Y. Wang, X. He, P. Gao, L. Feng and L. Zhang, *Environ. Res.*, 2024, **247**, 118301.
18 C. Y. Liang, J. Pan, A. M. Bai and Y. J. Hu, *Int. J. Biol. Macromol.*, 2020, **149**, 1118–1129.
19 K. Kasirajan, M. Karunakaran and H. K. Choi, *J. Environ. Chem. Eng.*, 2024, **12**(5), 113535.
20 M. Karim, A. Shokry, S. Ebrahim and M. Khalil, *Colloids Surf., A*, 2022, **652**, 129735.
21 S. Khan, A. Gupta, N. C. Verma and C. K. Nandi, *Nano Lett.*, 2015, **15**(12), 8300–8305.
22 V. Gude, A. Das, T. Chatterjee and P. K. Mandal, *Phys. Chem. Chem. Phys.*, 2016, **18**(40), 28274–28280.
23 D. Ananya, G. Venkatesh, R. Debjit and C. Tanmay, *J. Phys. Chem. C*, 2017, **121**, 9634–9641.
24 S. Khan, W. Li, N. Karedla, J. Thiart, I. Gregor, A. M. Chizhik, J. Enderlein, C. K. Nandi and A. I. Chizhik, *J. Phys. Chem. Lett.*, 2017, **8**(23), 5751–5757.
25 S. Khan, N. C. Verma, M. Chethana and C. K. Nandi, *ACS Appl. Nano Mater.*, 2018, **1**(2), 483–487.
26 A. Das, D. Roy, M. Mandal, C. Jaiswal, M. Ta and P. K. Mandal, *J. Phys. Chem. Lett.*, 2018, **9**(17), 5092–5099.
27 A. P. Demchenko, *Introduction to Fluorescence Sensing*, Springer International Publishing, Cham, 2020, pp. 357–399.
28 A. Das, E. V. Kundelev, A. A. Vedernikova, S. A. Cherevkov, D. V. Danilov, A. V. Koroleva, E. V. Zhizhin, A. N. Tsypkin, A. P. Litvin, A. V. Baranov, A. V. Fedorov, E. V. Ushakova and A. L. Rogach, *Light: Sci. Appl.*, 2022, **11**(1), 92.
29 N. Ghorai, S. Bhunia, S. Burai, H. N. Ghosh, P. Purkayastha and S. Mondal, *Nanoscale*, 2022, **14**(42), 15812–15820.
30 H. Swaminathan and K. Balasubramanian, *J. Appl. Phys.*, 2019, **126**(8), 084503.
31 T. Wang, Z. Tao, C. Qu, S. Wang and Y. Liu, *Analyst*, 2021, **146**(1), 283–288.
32 Q. Ma, J. Wang, Z. Li, X. Lv, L. Liang and Q. Yuan, *Small*, 2019, **15**(32), 1804969.
33 W. Wattanathana, N. Suetrong, P. Kongsamai, K. Chansaenpak, N. Chuanopparat, Y. Hanlumyuang, P. Kanjanaboos and S. Wannapaiboon, *Molecules*, 2021, **26**(17), 5410.
34 N. A. Piro, J. R. Robinson, P. J. Walsh and E. J. Schelter, *Coord. Chem. Rev.*, 2014, **260**, 21–36.
35 J. W. Stouwdam, G. A. Hebbink, J. Huskens and F. C. van Veggel, *Chem. Mater.*, 2003, **15**(24), 4604–4616.
36 F. Meiser, C. Cortez and F. Caruso, *Angew. Chem., Int. Ed.*, 2004, **43**(44), 5954–5957.
37 F. Vetrone, R. Naccache, V. Mahalingam, C. G. Morgan and J. A. Capobianco, *Adv. Funct. Mater.*, 2009, **19**(18), 2924–2929.
38 D. Sarkar, S. Ganguli, T. Samanta and V. Mahalingam, *Langmuir*, 2018, **35**(19), 6211–6230.
39 Q. Zhang, S. O'Brien and J. Grimm, *Nanotheranostics*, 2022, **6**(2), 184–194.
40 N. A. Hafez, E. Fadl, S. Ebrahim, M. Soliman and A. Shokry, *Ceram. Int.*, 2025, **51**, 34350–34364.
41 M. A. El-Naka, A. El-Dissouky, G. Y. Ali, S. Ebrahim and A. Shokry, *Talanta*, 2023, **253**, 123908.
42 G. Saber, G. Badie, A. El-Dissouky, S. Ebrahim and A. Shokry, *Advanced Quantum Technologies*, 2023, p. 2300154.
43 M. A. El-Naka, A. El-Dissouky, G. Y. Ali, S. Ebrahim and A. Shokry, *RSC Adv.*, 2022, **12**(52), 34095–34106.
44 P. Steliopoulos, *MethodsX*, 2015, **2**, 353–359.
45 S. Ebrahim, A. Shokry, M. M. A. Khalil, H. Ibrahim and M. Soliman, *Sci. Rep.*, 2020, **10**(1), 13617.
46 A. Abebayehu, *GSC Biol. Pharm. Sci.*, 2023, **22**(2), 001–013.
47 S. K. Tammina, D. Yang, S. Koppala, C. Cheng and Y. Yang, *J. Photochem. Photobiol., B*, 2019, **194**, 61–70.
48 C. Zhou, J. Song, L. Zhou, L. Zhong, J. Liu and Y. Qi, *J. Lumin.*, 2015, **158**, 176–180.
49 T. L. Tan, C. W. Lai and S. B. Abd Hamid, *J. Nanomater.*, 2014, **2014**(1), 371720.
50 Z. Zhang, J. Li, X. Wang, A. Liang and Z. Jiang, *Microchim. Acta*, 2019, **186**, 1–9.
51 M. Wang, R. Sun, Q. Wang, L. Chen, L. Hou, Y. Chi, C. H. Lu, F. Fu and Y. Dong, *Chem.–Eur. J.*, 2018, **24**(17), 4250–4254.

52 P. Brachi, *Appl. Catal., B*, 2020, **263**, 118361.
53 Y. Li, H. Meng, Y. Li, B. Pang, G. Luo and J. Huang, *New J. Chem.*, 2018, **42**(23), 18961–18968.
54 J. Upan, N. Youngvises, A. Tuantranont, C. Karuwan, P. Banet, P. H. Aubert and J. Jakmunee, *Sci. Rep.*, 2021, **11**(1), 13969.
55 C. Liu, F. Zhang, J. Hu, W. Gao and M. Zhang, *Front. Chem.*, 2021, **8**, 605028.
56 M. Mostafa, J. El Nady, S. M. Ebrahim and A. M. Elshaer, *Opt. Mater.*, 2021, **112**, 110732.
57 L. Liu, J. Zhang, Z. Yuan and G. Zhao, *Sens. Actuators, B*, 2023, **380**, 133320.
58 H. L. Tran and R. A. Doong, *Anal. Methods*, 2019, **11**(35), 4421–4430.
59 R. Adel, S. Ebrahim, A. Shokry, M. Soliman and M. Khalil, *ACS Omega*, 2021, **6**(3), 2167–2176.
60 J. F. Liu, H. D. Xian and G. L. Zhao, *Struct. Rep.*, 2009, **65**(6), m650.